Performance of a Reconfigurable Antenna Configuration Selection Scheme in a MIMO-OFDM System with Modulation Rate Adaptation

David Gonzalez, John Kountouriotis, Daniel Lach, Renan Bertolazzi, Pujashree Das, and Kapil Dandekar
Department of Electrical and Computer Engineering
Drexel University,
Philadelphia, PA 19104
Email: {dg345, jk368, dtl35, rab, pd48, dandekar}@drexel.edu

***Abstract*—In this paper we investigate the performance of an antenna configuration selection algorithm for a pattern reconfigurable antenna in a 2×2 MIMO-OFDM system. Channel capacity measurements were performed over a single link in both Line-of-sight (LOS) and Non-LOS (NLOS) indoor environments. From these measurements, an adaptive configuration selection algorithm was developed and the scheme's performance gains relative to a non-reconfigurable antenna were quantified. Finally, the configuration selection algorithm was also paired with a modulation rate adaptive scheme in order to exploit the improved channel capacity available with reconfigurable antennas.**

I. Introduction

Reconfigurable antennas are a promising addition to MIMO-OFDM systems due to their demonstrated ability to improve system performance. Reconfigurable antennas are capable of changing the propagation characteristics of a wireless channel by dynamically modifying their radiation properties [1]. This ability to switch between multiple radiation patterns can be an effective technique for improving the channel conditions between a transmitter and receiver [2].

Multiple researchers have suggested the use of switching algorithms to dynamically select configurations with the goal of maximizing SNR [1] or channel capacity [3]-[4]. This work extends these ideas into a practical algorithm for adaptive antenna configuration and modulation rate selection. Experimental performance of this joint antenna configuration and adaptive modulation technique is quantified and compared to both non-reconfigurable and optimal techniques.

The remainder of this document is organized as follows: descriptions of the software defined radio (SDR) platform and reconfigurable antenna arrays used in our experiments are provided in Section II. Sections III and IV detail the configuration selection and rate adaptation algorithms, respectively. Experimental results for LOS and NLOS scenarios are presented in Section V. Finally, conclusions are highlighted in Section VI.

II. Hardware

A. Software Defined Radio Testbed

Measurements were conducted using the Wireless Open-Access Research Platform (WARP) [5], a SDR testbed developed by Rice University. Displayed in Fig. 1, the WARP testbed is used to prototype physical (PHY) and medium access control (MAC) layer protocols [5]-[6]. Each WARP node used in our experiments was equipped with two radio cards and configured to operate in a 2×2 MIMO scheme. We made use of the WARPLab software development environment, a MATLAB API for rapid prototyping of PHY layer designs. WARPLab uses MATLAB in order to perform all of the PHY layer baseband processing. Processed baseband signals are then buffered on the WARP node for transmission over the air in real-time.

Fig. 1. Wireless Open Access Research Platform (WARP) Software Defined Radio

Our implementation of WARPLab uses spatial multiplexing and is based on the 802.11g OFDM frame format. The total bandwidth is divided into 64 subcarriers: 48 subcarriers are used for carrying data symbols, 4 carry pilot symbols for phase correction and tracking, and the remaining 12 are left unloaded to accommodate the carrier. Data can be modulated using four signal constellations: BPSK, QPSK, 16QAM, and 64QAM. Our WARP implementation also supports Forward Error Correction (FEC) convolutional coding with a coding rate of 1/2 serving as the base rate for all of our experiments. All packet transmissions consist of a 24 byte header (this includes a 2 byte header cyclic redundancy check (CRC)) modulated using BPSK as the base system rate. All packet payloads contained 1KB of data in addition to a 4 byte payload CRC. Packet payloads were modulated using the rate specified by the adaptive modulation scheme described in Section IV.

By nature, the WARPLab development environment pro-

978-1-61284-824-2/11/$26.00 ©2011 IEEE

vides centralized control of all WARP nodes connected to a single host PC. We take advantage of the availability of global knowledge at both ends of the communication link in order to avoid using an over-the-air (OTA) feedback mechanism that our antenna configuration and modulation rate selection algorithms would otherwise require. However, it is important to note that the selection algorithms discussed in this paper can be modified to operate using a Request-to-Send/Clear-to-Send (RTS/CTS) protocol in which RTS messages are used for collecting channel state information and the CTS messages are used for relaying required information back to the transmitter. Practical feedback and delay constraints will be considered in future work.

B. Reconfigurable Printed Dipole Arrays

The reconfigurable printed dipole arrays (RPDAs) used in our experiments were first introduced by the authors in [7]. RPDAs have beam configurations that can be electronically controlled by adjusting the length of each dipole antenna in the array. Multiple radiation patterns are generated as a result of varying levels of mutual coupling between array elements when the array geometry is changed [3]. Shown in Fig. 2, the RPDA uses PIN diode switches to achieve four distinct operating states. When the switches on an antenna are inactive, that antenna is said to be operating in a "short" configuration. Active switches cause an antenna to operate in a "long" configuration. The complete array at one end of the link uses a combination of the individual antenna states to form the following configurations: short-short, short-long, long-short, and long-long.

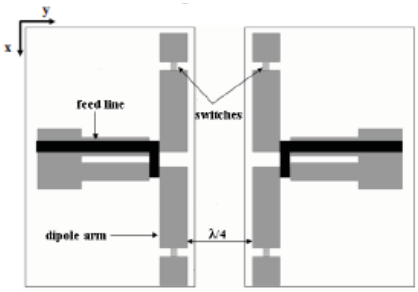

Fig. 2. Reconfigurable Printed Dipole Array

III. Configuration Selection Algorithm

We investigate the performance of a switching algorithm that selects configurations based on the achievable channel capacity for arrays deployed at both ends of a communication link. When calculating the channel capacity, a Frobenius normalization of the channel matrix is calculated on a per-subcarrier basis when the 'short-short' reference configuration is active at both the transmitter and receiver [7]. The 'short' configuration is used as the reference configuration because it is the most efficient in terms of radiation and matching [3]. The normalization factor, given by

$$N_F = \sqrt{\frac{||H_{short}||_F^2}{N_{Tx}N_{Rx}}} \tag{1}$$

removes the path loss from the different channel matrices and preserves the relative antenna gain effects of each configuration [7]. The channel capacity for a given configuration is then given by

$$C_j = \frac{1}{m}\sum_{i=1}^{m} log_2\left[det\left(I_{N_{RX}} + \frac{SNR}{N_{TX}}H_{ij}H_{ij}^H\right)\right] \tag{2}$$

where j is the antenna configuration, H_i is the normalized channel matrix for subcarrier i at configuration j, H^H is the Hermitian matrix of H, SNR is the post-processing SNR from the header of a successfully received packet, and m is the total number of subcarriers.

The antenna selection algorithm consists of two separate states. The first state consists of a training interval in which the capacity for each configuration is measured one packet at a time. This approach differs from the training method used in [1], by which antenna configurations were trained over a specially constructed frame of OFDM training symbols. Given constraints imposed by our use of WARPLab, switching antenna configurations over training symbols is not possible.

Each time a packet is received during the training interval, the receiver collects link statistics (i.e. post-processing SNR (PPSNR), channel matrices, packet error rates, etc.) and maintains a record of the antenna configuration that maximizes the channel capacity. The receiver also informs the transmitter of the array configuration and modulation rate (Section IV) that should be used in the next transmission. It is important to note that all packets transmitted during the training interval also contain 1KB payloads, so the configuration selection scheme does not sacrifice potential data transmission opportunities for the sake of training.

At the conclusion of the training interval, the selection scheme enters its next state by switching to the configuration that maximized the channel capacity during the training interval. When a new "best" antenna configuration is selected, the algorithm transmits two packets at this configuration before restarting a new training interval. Furthermore, each time the same configuration is selected following consecutive training intervals, the number of packets transmitted using this configuration is doubled before returning to the training state. By using this technique, it is possible for the nodes to make sustained use of a promising array configuration.

A particular challenge of using pattern reconfigurable antennas is the reduction in performance caused by stale channel state information and extensive configuration training [2],[8]. The goal of this work is to identify a selection technique that reduces the amount of training that is required for each antenna configuration. We show in Section V that for the RPDAs, certain configurations consistently perform better than others in a given link. By tracking the average channel capacity measured for each antenna configuration over multiple training intervals, a subset of the configurations can be eliminated from further training [4], thereby reducing the overall amount of training required and improving the long-term average channel capacity.

IV. Modulation Rate Adaptation

Pairing a modulation rate adaptive scheme with the configuration selection algorithm can further improve system performance by taking advantage of the increase in SNR to increase system throughput. A practical modulation rate selection scheme was implemented based on measuring the symbol estimation error variance for each successfully received packet header. The symbol estimation error variance is an adequate indicator for the performance of each of the available QAM rates because the same average power per symbol is applied to all of the rates.

Upon the successful reception of a packet header, as indicated by successfully passing the header CRC, the transmitted symbol stream is reconstructed to obtain the symbol estimation error variance. The symbol error variance is given by

$$\sigma^2 = E\{|\hat{s} - s|^2\} \tag{3}$$

where $\hat{s}$ is the estimated symbol and s is the transmitted symbol [9]. The transmitted symbol stream corresponding to the header is reconstructed because it is possible to successfully decode a packet even when a symbol is received in error due to use of convolutional coding.

The procedure detailed in [10] for relating the error probability for 16-QAM given noise power was extended to derive expressions for the remaining modulation rates (Table I). In each of these expressions, *N* is twice the symbol estimation error variance, and *d* is the distance between two adjacent points on the M-ary constellation diagram [10]. The distance *d* can be controlled in WARPLab such that the average symbol power for all modulation indices is equal to one. The expressions in Table I were used to develop a lookup table for choosing a modulation rate for a measured noise power such that a predetermined symbol error rate (SER) (i.e. 10^{-2} and 10^{-3} in LOS and NLOS scenarios, respectively) was satisfied. The SER is a good approximation of BER, by the assumption that the probability of a symbol being mistaken for a neighboring one is much greater than the probability of a symbol being mistaken for any other than the neighboring symbols. Different SER thresholds were used for LOS and NLOS in an attempt to achieve comparable throughput between scenarios. Given the gray coding that is applied, by wrongly estimating a symbol as being the neighboring one and not the original transmitted symbol, only one bit is in error [10].

TABLE I
Error Probability Expressions for Several M-ary QAM Modulations

M-QAM	P_{eM}	d
BPSK	$Q\left(\frac{d}{\sqrt{2N}}\right)$	2
4QAM	$2Q\left(\frac{d}{\sqrt{2N}}\right)$	1.4142
16QAM	$3Q\left(\frac{d}{\sqrt{2N}}\right)$	0.6324
64QAM	$\frac{7}{2}Q\left(\frac{d}{\sqrt{2N}}\right)$	0.3086

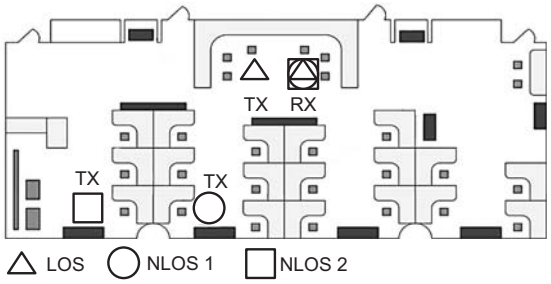

Fig. 3. Node placements in LOS and NLOS test scenarios.

Modulation rate adaptation is applied differently based on the state of the configuration selection algorithm. During a given training interval, the modulation rate applied to all packet payloads corresponds to the average PPSNR calculated for all configurations in the previous training interval. This approach is necessary since the receiver immediately switches to the next configuration upon the reception of a packet, so the channel state information collected for the current packet would not necessarily be valid for the next packet transmission. However, when a training interval is complete and the "best" configuration is selected, modulation rates are adjusted on a per-packet basis for as many transmissions as the best configuration is active.

Two performance metrics are available for evaluating the performance of the adaptive modulation scheme. Packet error rates (PER) are used to assess the overall link quality while over-the-air data rates measure the algorithm's ability to take maximize throughput.

V. Measurement Setup and Results

Measurements were taken in a typical indoor laboratory environment in the Drexel Wireless Systems Lab. A floor plan of the lab with node placements for each test is shown in Fig. 3. Three measurement positions were used in order to characterize the algorithm's performance in LOS and NLOS scenarios. For each position, two sets of measurements were taken. The purpose of the first set of measurements was to characterize each configuration's performance in terms of achievable channel capacity. This was accomplished by cycling through each of the 16 available configurations until 200 packets were transmitted using each configuration (this corresponds to a total of 3200 packet transmissions per test). Note that during these tests, the nodes were forced into a perpetual training state and no attempt was made to transmit at the "best" configuration identified for each training sequence. In addition, the modulation rate used for each packet during a given training interval corresponded to the average PPSNR measured during the previous training interval.

The achievable capacity for the RPDA is defined by the capacity yielded by the "best" configuration in each training interval [3]. The difference in capacity between the optimal configurations and the reference "short-short" configuration is used in order to quantify the performance gains of the RPDA relative to a non-reconfigurable antenna solution. Fig. 4 shows

the CDFs of the empirical channel capacities for the reference configuration and the optimal configurations. The CDFs for the reference configuration are drawn over the 200 packets made at the reference configuration. Similarly, the CDFs for the channel capacity at optimal configuration are obtained from the configurations that yielded the highest capacity during each training interval. Like the CDFs for the reference configuration, the CDFs for the optimal configuration are drawn over 200 packets. The largest capacity gain was realized in the LOS test scenario where an improvement of 27% was achieved. These results are directly in line with similar experiments using the RPDA conducted in previous work [3],[7].

Fig. 5 shows the average channel capacity for each configuration at all three node locations. For each location, the average capacity calculated over all 200 training intervals is compared to the average capacity taken over the first 10 training intervals. It is evident from this plot that for a given link, certain antenna configurations consistently yield higher channel capacity than others. Perhaps more importantly, the results from this figure indicate that for a given link, the performance of each configuration does not significantly change from one training interval to the next. In fact, the configurations identified as providing the highest average channel capacity after the 200th training interval could be identified after 10 training intervals.

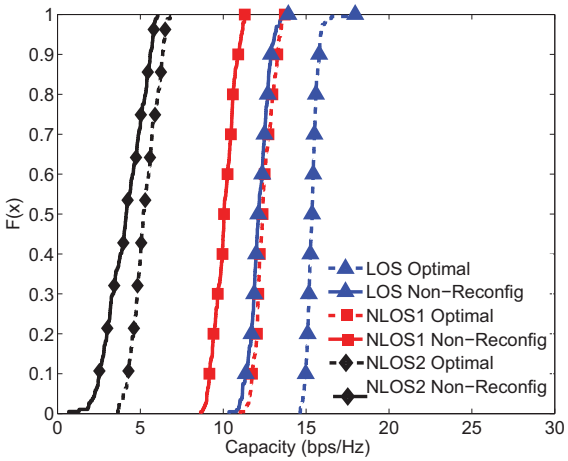

Fig. 4. Test 1 empirical channel capacity CDFs for non-reconfigurable and optimal configurations for each environment.

This result motivates the reduction of the overall set of array configurations that should be used in subsequent training intervals by only switching between configurations that consistently yield the highest capacity. Having the ability to eliminate configurations in this manner largely depends on the channel variability. In order to properly respond to large channel variations, a method for reinstating configurations and retraining over the complete set of configurations should be applied if the performance of the reduced set of configurations changes by some user-defined margin. The results shown so far, and those that follow indicate that the channel conditions remained fairly static over each of the tests. Amending the selection algorithm to handle wide channel variations will be considered in future work.

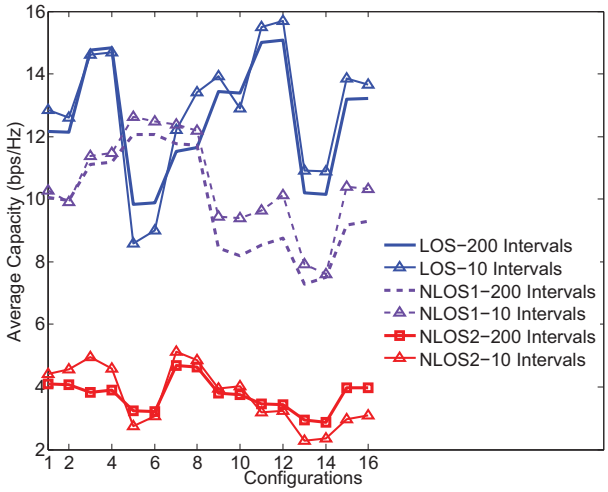

Fig. 5. Average capacity for each antenna configuration in Test 1 measurements.

In the second set of measurements, the complete antenna switching algorithm was implemented. That is, after each training interval, transmissions were made using the best configuration and modulation rates were selected on a per-packet basis for the duration of the transmissions at the best configuration. As in the first set of measurements, channel state information was collected over 3200 total transmissions. Drawing from the results from the first set of measurements that the long-term achievable capacity for each configuration can be approximated in relatively few antenna training intervals, after 10 training intervals, the number of configurations available to the nodes was reduced from 16 to 5. This reduced set included the top four configurations that achieved the highest average capacity after the 10 training intervals and the reference "short-short" configuration. The reference configuration was retained for calculating the normalization factor from (1) and to provide further comparison for the capacity and PPSNR achieved in the adaptive scheme and the non-reconfigurable case.

In Fig. 6, the empirical CDFs for the PPSNR from the LOS position are plotted for the reference configuration and for the switching algorithm. The values of PPSNR for the reference configuration are a compilation of measured PPSNR for all transmissions in which the short-short configuration was used at the transmitter and receiver. Similarly, the values for the switching algorithm were extracted from all of the transmissions made at configurations other than the reference configuration. These transmissions also include the packets sent during the first 10 training intervals prior to when the set of configurations available to the nodes was reduced. For this test, due to the proximity of the nodes, the PPSNR achieved by each configuration did not vary enough for the the selection algorithm to provide more than a negligible increase in PPSNR. Recall from Section III, the switching algorithm is designed to increase the number of transmissions

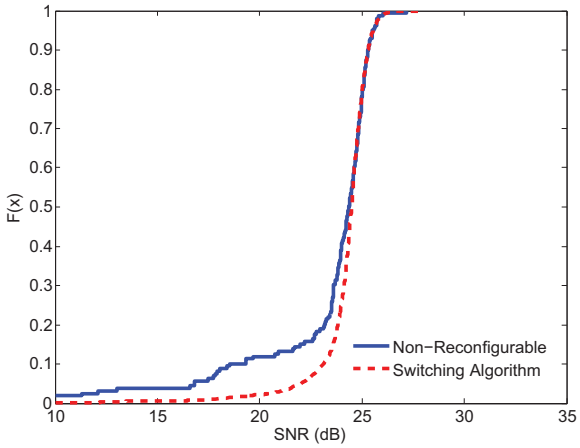

Fig. 6. Empirical PPSNR CDFs for non-reconfigurable and reduced set of configurations for LOS position.

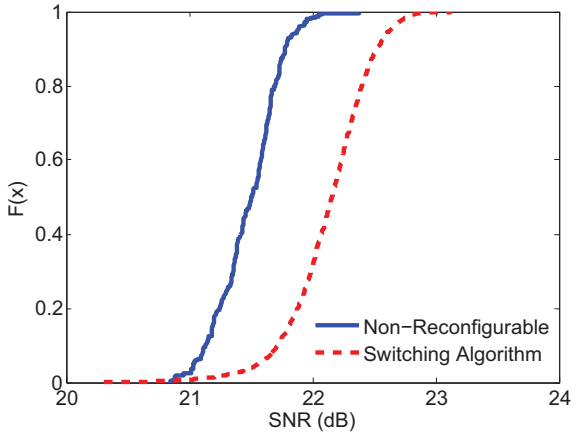

Fig. 7. Empirical PPSNR CDFs for non-reconfigurable and reduced set of configurations for NLOS position 1.

made at a configuration that is continuously selected at the conclusion of every training interval in order to reduce the amount of time the algorithm spends in the training state. This behavior can be seen in Table II where one particular configuration (Long-Long/Long-Short) was favored over the rest of the configurations. While this configuration provided a 4% increase in PPSNR over the reference configuration, the effect of training the remaining configurations reduced the overall average PPSNR and lowered the performance gains relative to the reference configuration. It is important to note that Table II shows the total number of transmissions made for each configuration after being selected as the best configuration following a training interval and the average PPSNR shown in the table is calculated over all transmissions and not just those shown in the table.

TABLE II
NUMBER OF PACKETS TRANSMITTED AT A GIVEN "BEST" CONFIGURATION FOR LOS SCENARIO

Configuration (Tx/Rx)	No. Packets	Average PPSNR (dB)
Short-Short/Short-Short	-	23.3
Long-Short/Short-Short	59	23.7
Long-Long/Short-Short	10	23.7
Long-Long/Long-Short	1956	24.5
Long-Long/Long-Long	258	24.2

For the first NLOS position, the configurations selected after the initial 10 training intervals are shown in Table III. For these measurements, two configurations were highly favored over the others with these two configurations producing nearly identical performance in terms of PPSNR. Although not implemented in the measurements discussed here, situations in which two or more configurations behave identically should be handled such that only one configuration is selected continuously in order to avoid the selection algorithm toggling between them. Doing so can eliminate unnecessary training intervals by extending the number of transmissions made by a single configuration. Fig. 7 shows the empirical CDFs of the PPSNR for the reference configuration and the selection scheme for the first NLOS position. The PPSNR achieved by the selection algorithm in this position was a modest increase of 3.7% over the reference configuration.

TABLE III
NUMBER OF PACKETS TRANSMITTED AT A GIVEN "BEST" CONFIGURATION FOR NLOS SCENARIO 1

Configuration (Tx/Rx)	No. Packets	Average PPSNR (dB)
Short-Short/Short-Short	-	21.5
Short-Short/Short-Long	6	22.2
Short-Long/Short-Long	2	22.2
Long-Short/Short-Long	914	22.3
Long-Long/Short-Long	922	22.3

The benefits of using the switching algorithm are most evident from the results obtained from the second NLOS position. As in the previous tests, Fig. 8 shows the empirical CDFs of the PPSNR for the reference configuration and the selection scheme. This position yielded the largest increase in PPSNR over the reference configuration at 33%. Once again, the configurations chosen at the conclusion of the first 10 training intervals are shown in Table IV. As was the case in the first NLOS position, multiple configurations behaved very similarly leading to a nearly even distribution of packets transmitted for three of the four selected configurations.

TABLE IV
NUMBER OF PACKETS TRANSMITTED AT A GIVEN "BEST" CONFIGURATION FOR NLOS SCENARIO 2

Configuration (Tx/Rx)	No. Packets	Average PPSNR (dB)
Short-Short/Short-Short	-	11.4
Short-Short/Short-Long	264	15.5
Short-Long/Short-Long	256	15.6
Short-Short/Long-Long	238	15.0
Short-Long/Long-Long	165	15.0

We conclude our discussion of the results by comparing the packet error rates and over-the-air data rates for all tests. As

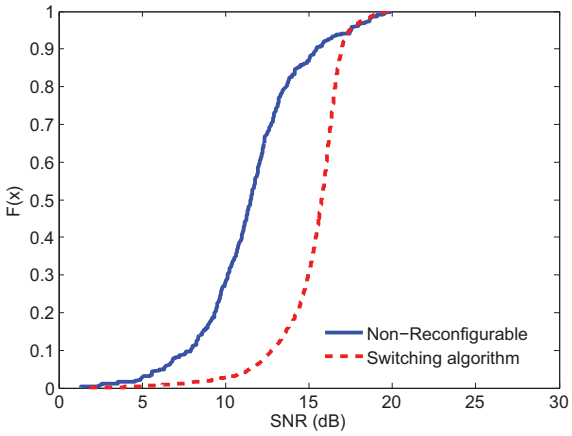

Fig. 8. Empirical PPSNR CDFs for non-reconfigurable and reduced set of configurations for NLOS position 2.

mentioned earlier, in the first set of measurements, modulation rate adaptation was performed based on the average PPSNR over one training interval. In the second set of measurements, modulation rate adaptation during the training intervals was performed as in the first set of measurements, however, modulation rate adaptation was also applied on a per-packet basis at the end of each training interval when transmissions at a best configuration were being made.

For the LOS measurements the OTA data rates were nearly identical across both sets of tests. In the first set of LOS measurements, the average PPSNR yielded by each configuration from one training interval to the next was large enough to apply 16-QAM for most of the transmissions over the duration of the experiment. This was also true for training intervals for the second set of measurements in the LOS position. Although modulation rate adaptation was to some extent allowed on a per-packet basis in the second set of measurements, the improvements in PPSNR at the best configurations made it possible to increase to the next modulation order (64-QAM) for only a fraction of the total transmissions. Furthermore, the PER measured for both tests indicate that the error probability constraint used to create the modulation index thresholds was too conservative for the given position.

In each of the NLOS positions, OTA data rates increased from the first set of measurements to the second. For the first NLOS position, The average PPSNR achieved in test 1 only allowed a maximum modulation rate of QPSK to be applied to most transmissions. In test 2, the average PPSNR for training intervals consisting of the reduced set of configurations made it possible for nearly all transmissions to be made at 16-QAM. In test 1 of the second NLOS position the data rate was hampered due to noisy channel conditions as indicated by the 15.4% PER. Measurements for this test were conducted during a time of high traffic in the Drexel Wireless Systems Lab and as a result, BPSK was the highest supported modulation rate for most of the transmissions.

TABLE V
PACKET ERROR RATES AND OTA DATA RATES FOR EACH NODE POSITION

Position	Metric	Test 1	Test 2
LOS	PER	0.22%	0.34%
	OTA Data rate (Mbps)	21.19	22.76
NLOS 1	PER	0.06%	0.03%
	OTA Data rate (Mbps)	11.66	21.29
NLOS 2	PER	15.4%	0.84%
	OTA Data rate (Mbps)	6.60	11.95

VI. CONCLUSIONS

A configuration selection algorithm based on increasing channel capacity using reconfigurable printed dipole arrays has been proposed. Adaptive modulation has been added to the system with reconfigurable antennas in order to exploit increases in PPSNR and increase throughput. In future work, we will investigate practical feedback mechanisms and analyze the effects of feedback delay on the configuration selection algorithm. Our current work has not proposed a method for reinstating configurations that have been removed following the initial cutoff training interval. Doing so is critical to improving the algorithm's performance in highly varying channels. Future work will focus on both the reinstatement criteria and the selection of the training interval cutoff. Finally, we will assess the algorithm's performance using similar reconfigurable antenna systems and explore practical protocols for configuration selection over multiple links.

ACKNOWLEDGMENTS

The work conducted in this project was supported by the National Science Foundation under grant 0916480.

REFERENCES

[1] A. Grau, H. Jafarkhani, and F. D. Flaviis, "A reconfigurable multiple-input multiple-output communication system," *IEEE Transactions on Wireless Communications*, vol. 7, no. 5, pp. 1719–1733, 2008.

[2] D. Piazza, J. Kountouriotis, M. D'Amico, and K. R. Dandekar, "A technique for antenna configuration selection for reconfigurable circular patch arrays," *IEEE Transactions on Wireless Communications*, vol. 8, no. 3, pp. 1456–1467, Mar. 2009.

[3] D. Piazza, N. J. Kirsch, A. Forenza, R. W. Heath, and K. R. Dandekar, "Design and Evaluation of a Reconfigurable Antenna Array for MIMO Systems," *IEEE Transactions on Antennas and Propagation*, vol. 56, no. 3, pp. 869–881, Mar. 2008.

[4] H. Pan, G. Huff, T. Roach, Y. Palaskas, S. Pellerano, P. Seddighrad, V. Nair, D. Choudhury, B. Bangerter, and J. Bernhard, "Increasing channel capacity on mimo system employing adaptive pattern/polarization reconfigurable antenna," in *Antennas and Propagation Society International Symposium, 2007 IEEE*, 2007, pp. 481 –484.

[5] Rice University WARP project. [Online]. Available: http://warp.rice.edu

[6] K. Amiri, Y. Sun, P. Murphy, C. Hunter, J. R. Cavallaro, A. Sabharwal, and M. St, "WARP , a Unified Wireless Network Testbed for Education and Research," *IEEE International Conference on Microelectronic Systems Education*, p. 1, 2007.

[7] D. Piazza and K. Dandekar, "Reconfigurable antenna solution for MIMO-OFDM systems," *Electronics Letters*, vol. 42, no. 8, pp. 446 – 447, 13 2006.

[8] D. Piazza, P. Mookiah, M. D'Amico, and K. Dandekar, "Experimental analysis of pattern and polarization reconfigurable circular patch antennas for MIMO Systems," *Vehicular Technology, IEEE Transactions on*, vol. 59, no. 5, pp. 2352 –2362, June 2010.

[9] C.-J. Ahn and I. Sasase, "The effects of modulation combination, target BER, Doppler frequency, and adaptation interval on the performance of adaptive OFDM in broadband mobile channel," *IEEE Transactions on Consumer Electronics*, vol. 48, no. 1, pp. 167–174, Feb. 2002.
[10] B. Lathi, *Modern Digital and Analog Communication Systems*, 3rd ed. New York, NY: Oxford University Press, 1998, ch. 14.